# *SLK* is mutated in individuals with a neurodevelopmental disorder

Lama Alabdi,[a,k] Norah Altuwaijri,[a,k] Jun-yi Zhu,[b,k] Stephanie Efthymiou,[c] Hangnoh Lee,[b] Jianli Duan,[b] Israa Salem,[d] Piao Yu,[d] Nor Linda Abdullah,[d] Fatema Alzahrani,[a] Qing Xu,[e] Mashael M. Felemban,[e] Abdullah Alfaifi,[f] Fatima Rahman,[g] Marilena Christoforou,[c] Shazia Maqbool,[g] Julian A. Martinez-Agosto,[h] Hessa S. Alsaif,[i] Mais Hashem,[a] Rana Helaby,[a] Ahood Alsulaiman,[a] SYNaPS Study Group,[c,l] Queen Square Genomics,[c] Reza Maroofian,[c] Henry Houlden,[c] Stefan T. Arold,[d,e] Leena A. Ibrahim,[d,e] Zhe Han,[b,**] and Fowzan S. Alkuraya[a,j,*]

[a]Department of Translational Genomics, Genomic Medicine Centre of Excellence, King Faisal Specialist Hospital and Research Center, Riyadh, 11211, Saudi Arabia
[b]Center for Precision Disease Modeling, Division of Endocrinology, Diabetes and Nutrition, Department of Medicine, University of Maryland School of Medicine, 670 West Baltimore Street, Baltimore, MD, 21201, USA
[c]Department of Neuromuscular Disorders, UCL Institute of Neurology, Queen Square, London, WC1N 3BG, UK
[d]KAUST Center of Excellence for Smart Health, Biological and Environmental Science and Engineering Division, King Abdullah University of Science and Technology (KAUST), Thuwal, 23955-6900, Saudi Arabia
[e]KAUST Center for Smart Health, King Abdullah University of Science and Technology (KAUST), Thuwal, 23955-6900, Saudi Arabia
[f]Department of Pediatrics, Security Forces Hospital, Riyadh, 12611, Saudi Arabia
[g]Developmental & Behavioral Paediatrics, Institute of Child Health and the Children Hospital, Lahore, 54600, Pakistan
[h]Departments of Human Genetics, Pediatrics and Psychiatry, David Geffen School of Medicine at UCLA, Los Angeles, CA, 90095, USA
[i]Wellness and Preventative Medicine Institute, Health Sector, King Abdulaziz City for Science and Technology (KACST), Riyadh, 11442, Saudi Arabia
[j]Lifera Omics, Riyadh, 13519, Saudi Arabia

eBioMedicine
2025;116: 105725
Published Online xxx
https://doi.org/10.1016/j.ebiom.2025.105725

## Summary

**Background** Key to neuronal cell polarization and maturation is proper cytoskeletal organization and function that endows the bipolar neuronal cell with mature dendrites, axons, and functional synapses. Ste20-like kinase (SLK) has been shown to have various cytoskeletal roles. SLK regulates the polarity of microtubules, and its deficiency in the developing murine cortex leads to major defects including impaired development of the distal dendritic tree. No neurodevelopmental phenotypes in humans, however, have been linked to *SLK*.

**Methods** Clinical phenotyping, positional mapping, exome sequencing and functional analyses using patient-derived cells, *SLK* knock down cell lines, as well as a *Drosophila* model of Slik deficiency (the orthologue of *SLK*).

**Findings** We identified three individuals from three families (two are consanguineous) in whom a neurodevelopmental disorder (NDD) is linked to biallelic variants in *SLK*. The deleterious nature of these variants is confirmed by their failure to rescue the abnormal synapse maturation and locomotor defects phenotype in a *Drosophila* model of Slik deficiency. We also recapitulated the previously published abnormal cytoskeletal phenotype using patient cells, which showed abnormal organization of the cytoskeleton with accompanying impairment of migration and polarization. Furthermore, transdifferentiated neurons from patient fibroblasts displayed immature neuronal-like morphology with reduced dendritic arborization.

**Interpretation** Our results support an autosomal recessive *SLK*-related NDD and suggest abnormal cytoskeleton-mediated neuronal maturation as the underlying mechanism.

**Funding** MRC (MR/S01165X/1, MR/S005021/1, G0601943, MR/S005021/1), The National Institute for Health Research University College London Hospitals Biomedical Research Centre, Rosetree Trust, Ataxia UK, MSA Trust, Brain Research UK, Sparks GOSH Charity, Muscular Dystrophy UK (MDUK), Muscular Dystrophy Association (MDA USA). National Institutes of Health (NIH) grants HL134940 and DK098410. King Abdullah University of Science and Technology (KAUST) through the baseline fund to STA and LI as well as to STA and LI, and the KAUST Center of Excellence for Smart Health (KCSH), under award number 5932.

*Corresponding author. Lifera Omics, Innovation Boulevard St, KAFD, Al aqeeq Dist KAFD, 4.07, 5th Floor Riyadh 13519-3004, Saudi Arabia.
**Corresponding author.
*E-mail addresses:* falkuraya@liferaomics.com.sa (F.S. Alkuraya), zhan@som.umaryland.edu (Z. Han).
[k]Indicate authors who contributed equally.
[l]The members of steering committee and collaborative group are listed in the Supplementary Material.

Keywords: SLK; Neurodevelopmental disorder; Transdifferentiation; Focal adhesion

## Research in context

### Evidence before this study

The role of Ste20-like kinase (SLK) in cytoskeleton organization through the polarization of microtubules has been shown in several studies. The function of SLK is exerted through its activation and recruitment to focal adhesions which are critical for filapodial extension and cytoskeletal remodelling, and ultimately cell migration. *Slk* knockout in mice results in embryonic lethality; however, targeted knockdown of *Slk* in the developing mouse cortex results in developmental defects of the distal dendritic tree. These and other studies strongly suggest that SLK plays a critical role in development of the nervous system in mammals.

### Added value of this study:

After identifying a compelling variant in a gene (*SLK*) in a patient with a neurodevelopmental disorder, we used the GeneMatcher platform and Lifera Omics Database to identify three additional families with similar phenotypes and convincing biallelic variants in the same gene. Two of these families were recruited and included in our analysis. We have provided evidence supporting the role of SLK in human neuronal development and showed that SLK deficiency results in defects in neuronal morphologies (which could impact their function) as well as focal adhesions. We also showed that Slik deficiency in the *Drosophila* model resulted in abnormal synapse maturation and locomotor defects phenotype that we failed to rescue by expressing the variants identified in our human patients.

### Implications of all the available evidence

Our data support a link between deleterious variants in *SLK* and neurodevelopmental phenotypes in humans. We also demonstrate that defects in cytoskeleton-mediated neuronal maturation may be the underlying mechanism of pathology.

## Introduction

Normal brain function relies on the proper establishment of the density, morphology, and spatial distribution of dendrites.[1] Normal dendrite development involves three recognizable stages: initiation, outgrowth/guidance, and branching (arborization).[2] Although much has been learnt about the factors that drive these processes, our knowledge about the molecular control of dendrite development remains incomplete. Key to dendrite development is the dynamic reorganization and turnover of the cytoskeleton. For example, microtubules with their associated motor proteins ensure normal antero- and retrograde transport of cargo between developing dendrites and cell body (soma), including neurotransmitters, receptors and signalling molecules.[3] Dendritic spines have been proposed as the key site of synaptic plasticity, and actin has been shown to play a major role in the development of dendritic spines as well as in endowing mature synapses with structural plasticity.

Phosphorylation plays a wide-ranging role in the dynamic control of the cytoskeletal architecture. The list of kinases and their targets that affect remodelling of the cytoskeleton during dendrite development is long and continues to grow. Examples include phosphorylation of WAVE1 that influences dendritic spine morphology by regulating actin polymerization, phosphorylation of β-tubulin by DYRK1A to modulate microtubule dynamics and regulate dendrite morphogenesis, and the mediation of dendritic spine maturation through TAOK2 kinase phosphorylation of Septin-7.[4] Abnormal phosphorylation can be expected to have profound deleterious effects on dendrite structure and function.

Ste20-like kinase (SLK) is a member of the GCK-V subgroup of Ste20-kinase family. The role of SLK in the cytoskeleton has been studied extensively. SLK has been shown to regulate the polarity of microtubules and their interaction with actin and the polymerization of F-actin.[5,6] SLK is activated and recruited to focal adhesions (FAs) whose assembly and reassembly, which involve filapodial extension and cytoskeletal remodelling, generate the contractile forces required for cell migration.[7,8] Until recently, the role of *SLK* in the nervous system has been limited to expression analysis showing marked enrichment in the developing brain despite an overall ubiquitous expression pattern.[9,10] The *Slk* knockout mouse could not be assessed for brain defects because of embryonic lethality.[11] To overcome this limitation, a recent study resorted to electroporation of shRNA in the developing mouse cortex, which led to impaired development of the distal dendritic tree.[12] This suggests that slk plays an important role in dendrite development in mammals although whether this applies to humans remains unknown. In this study, we report three affected children with a neurodevelopmental disorder (NDD) that segregates with likely deleterious recessive variants in *SLK*.

## Methods

### Human subjects and research ethics

The three families presented for genetic counselling because of the occurrence of global developmental delay

and intellectual disability and were subsequently recruited with informed written consent under institutional review board (IRB)-approved research protocols (KFSHRC RAC#2121053, UCL IRB # 22/NE/0080, and UCLA IRB #12-000989). Consent was also obtained from the families to publish identifiable images of the affected individuals.

### Genotyping and exome sequencing

Genome-wide genotyping was performed for Family 1 on the Axiom platform according to the manufacturer's instructions. Regions of homozygosity (ROH) > 2 Mb were used as surrogates of autozygosity using autoSNPs. Exome sequencing and subsequent filtering of variants by the candidate autozygome coordinates were performed for the index individuals in each family as described.[13] Exome sequencing was performed for Family 2 as previously described.[14]

### Cell culture and wound-induced cell migration assay

A sub-confluent fibroblast cell line derived from Family 1_IV:1 (validated by confirming the presence of the homozygous *SLK* variant and checked for mycoplasma contamination), wildtype fibroblasts (derived from healthy newborn males during circumcision procedures and validated by the absence of the *SLK* variant and checked for mycoplasma contamination), and transduced cells were all maintained in Minimum Essential Medium Eagle (MEM) supplemented with 10% foetal bovine serum (FBS, Gibco), 2 mM L-glutamine (Gibco) and penicillin G (200 U $ml^{-1}$, Gibco) in a humidified 37 °C incubator at 5% $CO_2$. For migration assays, fibroblasts were plated on 6-well cell culture plates pre-coated with 0.01% Poly-L-lysine (Sigma–Aldrich P4707) then serum starved overnight (MEM + 0.5% FBS). Cells were then washed with 1X PBS, incubated in MEM containing 10% FBS, scratch wounded with a pipette tip in the midline and allowed to migrate for the specified time points; 0, 4, 10, and 29 h. Independent triplicate experiments were performed, and representative images are shown. The percent wound closure and area of the wound were measured using the ImageJ plugin Wound healing size tool image tool analysis (https://github.com/AlejandraArnedo/Wound-healing-size-tool/wiki).[15]

### Antibodies and immunofluorescence

For immunofluorescence studies, fibroblast cells were plated on 0.01% Poly-L-lysine pre-coated coverslips, scratch wounded in the midline with a pipette tip, allowed to migrate for 2–3 h and fixed with 100% methanol for 20 min at –20 °C. Then, cells were rinsed with 1X PBS, blocked with 1 g bovine serum albumin +25 ml 1X PBS +2 ml goat serum and 0.1% Triton X-100 for 1 h and incubated overnight with either Anti-α-tubulin (ab7291) and Anti-pericentin (ab4448) or Anti-Giantin (ab37266). Antibodies were detected with either Goat Anti-Mouse IgG (H + L), FITC, Invitrogen (cat#62-6511) or Goat Anti-Rabbit IgG (H + L), Rhodamine (cat#31686) secondary antibodies. Vectashield mounting medium containing DAPI (H1200) was applied on all labelled coverslips. Golgi orientation was scored based on the direction of Giantin stain relative to the wound direction. Paralellness of microtubules was measured using the LPX ImageJ plugin (https://lpixel.net/services/research/lpixel-imagej-plugins/).[16] The total area of Golgi was manually measured using the ImageJ software. The directional orientation of Golgi was assessed visually and presented as percent mean polarization.

For Paxillin and Vinculin, glass-bottom dishes (Willco, #HBST-3512) were coated with 0.75 mg/ml Fibronectin (Fisher Scientific, #11564466) for 2 h at room temperature (RT). Trypsinized fibroblasts were then seeded onto the dishes for 2 h at RT and fixed with 4% paraformaldehyde (PFA) for 10 min. After fixation, cells were permeabilized with 0.1% Triton-X100 in PBS (PBST) for 30 min at RT and blocked with a 1% BSA solution in PBST for 1 h at RT. Following blocking, cells were incubated overnight at 4 °C with primary Paxillin antibody (5H11, #AHO0492), followed by a 1 h incubation with the secondary antibody (ab6563) at RT. Cells were then cultured continuously with AF-488 Vinculin (Abcam, #ab196454) overnight. Throughout each step, cells were washed three times with PBS. The resulting samples were observed under the Leica Stellaris Falcon.

### Isolation of focal adhesion proteins

To isolate focal adhesions from fibroblast cells, 10 cm culture plates were coated with 5 ml of 10 µg/ml human fibronectin or 10 µg/ml Poly-D-Lysine for 2 h. After washing, plates were blocked with 5 ml of 1% BSA in PBS for 30 min. Fibroblast cells, trypsinized and resuspended in serum-free DMEM, were seeded onto the coated plates and incubated for 2 h at 37 °C. Crosslinking was performed using 5 ml of 1.85 mg/ml DTBP in DMEM with 25 mM HEPES for 5 min, followed by quenching with 150 µL of 1 M Tris·Cl, pH 8. After removal of the crosslinking medium, plates were washed with cold PBS. Cell lysis was achieved by adding 5 ml of modified RIPA buffer (50 mM Tris·Cl, pH 7.6 150 mM NaCl 5 mM disodium EDTA, pH 8 2.5% (w/v) SDS 1% Triton X-100 1% sodium deoxycholate) per plate. The efficiency of cell lysis was observed under a microscope, and plates were washed to remove cell bodies. The lysed cells were treated with 100 µL of adhesion recovery solution (125 mM Tris·Cl, pH 6.8, 1% SDS, 150 mM DTT). The scraped solution was collected and stored in vials with 4 volumes of –20 °C acetone at a –80 °C freezer for subsequent mass spectrometry analysis.

### Sample preparation for LC-MS/MS analysis

The Filter-Aided Sample Preparation (FASP) method for processing SDS-solubilized cells involves preparing fresh solutions of UA (8 M Urea in 0.1 M Tris·Cl, pH

8.5), UB (8 M Urea in 0.1 M Tris·Cl, pH 8.0), 0.01 M DTT in UA, 0.05 M iodoacetamide (IAA) in UA, and 0.05 M NH4HCO3 (ABC). Isolated focal adhesion solutions were centrifuged, and protein pellets were resuspended in –20 °C acetone, followed by drying. To dissolve dried pellets, 30 µL of adhesion recovery solution was added. The dissolved pellets were mixed with 400 µL of UA in a 10 kDa centrifugal filter unit, centrifuged, and treated with DTT. After centrifugation, IAA was added, followed by UB, and centrifugation steps. ABC with trypsin was added, mixed, and incubated overnight. On the second day, filter units were centrifuged, treated with 0.5 M NaCl, and centrifuged again. Trifluoroacetic acid (TFA) was added (0.1%), followed by centrifugation. The filtrate was acidified with 0.1% TFA, desalted using OMIX C18 tips, dried, and stored at –20 °C for MS detection. For MS analysis, the Fusion Lumos mass spectrometer with EasySpray was used, applying an electrospray potential of 1.9 kV and a constant ion transfer tube temperature of 270 °C. Standard Mass spectrometry was performed using standard parameters for peptide analysis.

### Western blot analysis

Cells were lysed in RIPA buffer and lysates were cleared by centrifugation at 14000 rpm for 20 min at 4 °C. Protein concentrations were determined using protein assay dye reagent (Bio-Rad). Equal amounts of protein (20–40 mg) were electrophoresed on graduated 4–12% polyacrylamide gels (Invitrogen NP0335BOX) and transferred to PVDF membranes. Membranes were probed with the indicated antibodies overnight (Anti-SLK antibody (ab226986- RRID: AB_3675876) and Anti- GAPDH (ab8245-RRID:AB_2107448) at 4 °C in 5% BSA or skim milk powder in 1X PBS + 0.1% TWEEN 20. Target proteins were detected with horseradish peroxidase-coupled secondary antibodies combined with chemiluminescence (SuperSignal West Pico Mouse IgG Detection Kit #34082).

### RT-PCR and quantitative RT-PCR

For RT-PCR total RNA from Family 1_IV:1 and a control individual's fibroblast cell line were extracted with the QIAamp RNA Mini Kit (QIAGEN) according to the manufacturer's recommendations. Preparation of the cDNA was carried out with the iScriptTM cDNA synthesis kit and Poly T oligonucleotide primers (Applied Biosystems). Primers for *SLK* cDNA were designed for specific amplification (*SLK* exons 4–7). The two samples were run alongside *GAPDH* as an internal positive control. Relative quantitative RT-PCR for the expression of *SLK* was performed with SYBR Green and Applied Biosystems StepOnePlus Real-Time PCR System (StepOne$^{Tm}$ Software).

### Transdifferentiation protocol

The method used for the neural programming was slightly modified from a previously published protocol.[17] Prior to transduction, cells were seeded in a 24 well plate coated with 0.1% gelatin (Merck, Millipore): Control = $2.8 \times 10^4$ and SLK KO = $3.6 \times 10^4$ cells per well (The initial cell numbers were raised for *SLK* KO cells due to low number of cells that recovered post dissociation step (Day 10). One day post seeding of the Control and *SLK* KO fibroblasts and three days post *SLK* shRNA knockdown transduction, the fibroblasts were transduced with a lentivirus encoding *Ascl1* and *Brn2* (U6REST1_U6REST2.hPGK.BRN2.hPGK.Ascl1WPRE, Addgene # 101852) (2.71 × 108 IFU/ml) (Lentivirus packaging, GenScript). Polybrene 8 µg/ml and 1 µL of the lentivirus was added to the well and left to incubate for overnight. The media was changed the next morning and cells were observed. Three days after viral transduction, the media was replaced with fresh media (Ndiff227, Takara Bio) containing neural differentiation supplements LM22A4 (2 µM, R&D system), GDNF (2 ng/ml, R&D system), NT3 (10 µg/ml, R&D system), db-cAMP (0.5 mM, Sigma), CHIR99021 (2 µM, Sigma), SB-431542 (10 µM, Merck, Millipore), Noggin (0.5 µg/ml, R&D system), LDN-193189 (0.5 µM, Axon Med Chem) and Valproic acid sodium salt (1 mM, Sigma). The media was changed at half volume every 2–3 days. In preparation of cell replating, clean coverslips were coated with Polyornithine (15 µg/ml, Sigma) and Fibronectin (0.5 µg/ml, VWR) mixture overnight, rinsed with autoclaved distilled water thoroughly. The coverslips then were incubated in laminin (5 µg/ml, ThermoScientific) for 2 h. Ten days post viral transduction, the cells were replated onto the freshly coated coverslips in 24 well plates with media (Ndiff227, Takara Bio) and supplements LM22A4 (2 µM, R&D system), GDNF (2 ng/ml, R&D system), NT3 (10 µg/ml, R&D system) and db-cAMP (0.5 mM, Sigma). Laminin was added to the media to encourage cell attachment. The cultured cells were fixed at Day 12 post transduction with 4% paraformaldehyde (Sigma).

### Image acquisition and analysis of transdifferentiated cells

The images were captured using a confocal microscope, Zeiss LMS800 with AiryScan. All the measurements were carried out using ImageJ. The measurements include neurite length, neurite number, cell body diameter, number of nuclei and clusters and the size of the clusters. Neurite length was traced from the cell body until the next cell body and quantified using ImageJ. The Cluster's perimeter was traced and quantified. Each cluster was measured by the perimeter and Feret's diameter (which is the longest distance between any two points along the selection boundary, also known as maximum calliper). Cluster size (perimeter or Feret's diameter) were normalized either by the total measured area or the percentage measured area.

### *SLK*-shRNA lentivirus production

*SLK* Human shRNA plasmid kit (Locus ID 9748, Cat.# TL320620, OriGene) was used for generating shRNA

lentivirus to perform silencing of the *SLK* gene in fibroblasts. The 293FT cells (Thermo Fisher Scientific, #R70007) were cultured in Dulbecco's Modified Eagle's medium with high glucose, GlutaMAX Supplement (Thermo Fisher Scientific, #10564-029),10% foetal bovine serum, penicillin (100 units/ml) and streptomycin (100 μg/ml). The cultures were incubated at 37 °C in a humidified atmosphere containing 5% CO2. For Lentivirus production, 293FT cells were seeded in one 15-cm dishes without antibiotics for close to 24 h and co-transfected with the following plasmids using Polyethylenimine (150 μg/dish, Polysciences, #23966-1): psPAX2 (Addgene plasmid #12260, 27.6 μg/dish), pMD2.G (Addgene plasmid #12259, 8.3 μg/dish), and the *SLK*-shRNA expression vector (28.4 μg/dish). Four shRNA vectors pGFP-C-shLenti-*SLK*-shRNA and one scramble shRNA vector were used (OriGene Technologies, Inc. #TL320620 and #TR30021). The culture media were changed after 8 h of transfection, and then collected and combined in day 2, day 3 and day 4 after transfection. The media were cleared by filtration with 0.22 μm PES filter (Millipore, #S2GPT02RE) and concentrated by ultracentrifugation with Type 70 Ti rotor (Beckman Coulter, #337922) at 40,000 RPM for 1 h at 16 °C. The lentivirus was resuspended in Hanks' Balanced Salt Solution (HBSS, Thermo Fisher Scientific, #14025092). The viral titre obtained was 5 E+07 vg/μL.

### shRNA transduction in wild-type fibroblasts

*SLK*-shRNA lentiviral transduction was performed to knock down the *SLK* gene in wild-type (WT) fibroblasts. Cells were seeded in a 12-well plate 24 h before transduction, aiming for 60–70% confluency at the time of infection. On the day of transduction, three types of *SLK*-shRNA lentiviral particles, labelled shRNA A, shRNA B, and shRNA C, were thawed on ice for infection. In a separate Eppendorf tube, a transduction mixture was prepared by adding 1 ml of fresh complete medium containing polybrene at a final concentration of 2 μg/ml. The mixture was gently vortexed and subsequently added to each well of the 12-well plate. Cells were incubated with polybrene for 30 min at 37 °C in a humidified incubator with 5% $CO_2$ to enhance transduction efficiency. Following this incubation, 9 μL of viral particles were added directly to each well, and the plate was returned to the incubator. After 24 h of infection, the viral-containing medium was carefully removed, and cells were cultured in fresh, virus-free complete medium to support continued growth. To monitor the efficiency of transduction, cells were regularly observed for GFP expression, which was encoded by the shRNA construct. GFP expression served as a reporter, providing visual confirmation of successful viral integration. We then proceeded to perform transdifferentiation of the *SLK*-deficient fibroblasts as described above.

### Immunofluorescence

Cells on coverslips were rinsed with PBS, fixed with 4% PFA, rinsed with PBS and followed by permeabilization with 0.1% PBST. The cells were incubated in 10% serum, 0.3% Triton® X-100 in PBS. Cells were then incubated overnight with antibody in the buffer containing 1% BSA, 5% serum and 0.3% Triton® X-100 in PBS. Primary antibodies used mouse anti-MAP2 (EMD Millipore Corp, MAB3418, 1:250), mouse anti-TU-20 (EMD Millipore Corp, MAB1637, 1:250), chicken anti-GFP (Abcam, ab13970, 1:1000), guinea pig anti-NeuN (EMD Millipore Corp, ABN90P, 1:100), rabbit anti-SLK (Abcam, ab226986, 1:500) and DAPI. Cells were washed with PBS, incubated with secondary antibodies, washed with PBS and mounted.

### *Drosophila* lines

*Drosophila* stocks were obtained from the Bloomington Drosophila Stock Center (BDSC; Indiana University Bloomington, IN). Experiments employed the lines UAS-*Slik*-RNAi (BDSC IDs: 35179 and 55626), and *Slik* Trojan-Gal4 (BDSC ID: 83260). w1118 flies served as wild-type control. The elav-Gal4 (BDSC ID: 8765) driver was used to drive UAS-*Slik*-RNAi (BDSC IDs: 35179 and 55626) to silence *Slik* specifically in the fly nervous system. The *Slik* Trojan-Gal4 (BDSC ID: 83260) and UAS-GFP (BDSC ID: 6874) were used to visualize the expression pattern of Slik in the fly ventral ganglion.

### Generation of transgenic Drosophila carrying SLK wildtype and disease variants

The cDNA corresponding to human wildtype *SLK* (GenBank accession no. NM_014720.2) was obtained from Dr. Shinya Yamamoto, Baylor College of Medicine. Amino acid sequence "VINEVEKAPKELRKEL MKRRKEELAQSQHAQ" was deleted to generate the SLK transcript (NM_00134732.2). Next, oligonucleotide primers were designed to introduce the respective mutant sites using the Q5® Site-Directed Mutagenesis Kit (New England Lab, Inc; #E0554S), according to the manufacturer's instructions. The human reference, wildtype *SLK* and patient-derived variants were assembled into the pUAST attB vector. The transgenes were introduced into a fixed chromosomal docking site by germ line transformation to generate transgenic flies.

### Imaging the *Drosophila* brain and neuromuscular junction (NMJ)

Fly larval brains were dissected and fixed for 10 min in 4% paraformaldehyde 1X PBS and blocked for 40 min in 2% bovine serum albumin and 0.1% Triton X-100 in 1X PBS. Fluorescein (FITC) Goat anti-horseradish peroxidase (HRP) (Jackson ImmunoResearch Laboratories, Inc.) was incubated at 1:1000 dilution overnight at 4 °C. Confocal imaging was performed using a ZEISS LSM900 microscope with a 20 × Plan-Apochromat 0.8 N A. air objective. For quantitative comparisons of

fluorescence intensity, control groups were imaged first to establish the laser intensity and exposure time used for the entire experiment. The exposure time was based on image saturation (at a set point of approximately 70% of maximum saturation). ImageJ software (version 1.49) was used to process the images. We obtained images for six flies of each genotype.

Fly larval NMJs were dissected and fixed for 10 min in 4% paraformaldehyde 1X PBS and blocked for 40 min in 2% Bovine serum albumin and 0.1% Triton X-100 in 1X PBS. Mouse anti-CSP (Developmental Studies Hybridoma Bank; 6D6) was incubated at 1:1000 dilution overnight at 4 °C, followed by incubation with Cy3-conjugated secondary antibody (Jackson ImmunoResearch Laboratories, Inc.) and FITC goat anti HRP (Jackson ImmunoResearch Laboratories, Inc.) at 1:1000 dilution for 2 h at room temperature. Confocal imaging of NMJ 4 at Segment A5 was performed using a ZEISS LSM900 microscope with a 63 × Plan-Apochromat 1.4 N.A. oil objective. For quantitative comparisons of fluorescence intensity, control groups were imaged first to establish the laser intensity and exposure time used for the entire experiment. The exposure time was based on image saturation (at a set point of approximately 70% of maximum saturation). ImageJ software (version 1.49) was used to process the images. We obtained images for six flies of each genotype.

### Analysis of locomotion in larvae and adult flies

Larval locomotion was investigated by the larval righting assay. In this assay, each larva was placed on its dorsal surface, then the time taken to return to its ventral side was measured. At least 20 larva per genotype were analysed. Climbing male flies were monitored by analysing their ability to climb 6 cm within 14 s. A successful attempt was scored as 1, and failure to reach the top in time as 0. Each fly was assessed three times to calculate the average climbing score. At least 40 flies per genotype were analysed.

### *Drosophila* survival assay

*Drosophila* larvae were kept at 25 °C to enhance the UAS-transgene expression. Adult male flies were subsequently maintained in vials at 25 °C, each vial containing 20 animals. Mortality was monitored every 48 h. Per genotype, 100 flies were assayed. The survival curves for each genotype were constructed using actual data, not estimates.

### Statistical analysis

Statistical analyses for transdifferentiated cells were performed using GraphPad Prism for Windows. Analysis between 2 separate samples was evaluated using Mann–Whitney U test. This test was used for independent samples without a Gaussian distribution. Comparison between the three cell types, Unpaired t-test was used and one-way Analysis of Variance (ANOVA) was used only for neurite length measurement due to uneven number of neurites between the 3 cell types. A p-value of <0.05 was considered statistically significant. Quantitative data were plotted as mean ± standard deviation.

Statistical analyses for the fly work were performed using PAST.exe software (Natural History Museum, Norway). Values are presented along with the standard deviation. Data will be first tested for normality by using the Shapiro–Wilk test (a = 0.05). Normally distributed data were analysed either by Student's t-test (two groups) and Bonferroni comparison to adjust the p-value or by a one-way analysis of variance followed by a Tukey–Kramer post-test for comparing multiple groups. Nonnormal distributed data were analysed by either a Mann–Whitney test (two groups) and Bonferroni comparison to adjust p-value or a Kruskal–Wallis H-test followed by a Dunn's test for comparisons between multiple groups. Survival assay was analysed by Log–Rank test. All the analysis units were independent. Statistical significance was defined as p *<0.05, **<0.01, ***<0.001.

Statistical summaries and tests can be found in Table S3.

### Role of funders

Funders did not have any role in the study design, data collection, data analyses, interpretation, or writing of this manuscript.

## Results

### Identification of loss of function variants in *SLK* in patients with NDD

As part of our ongoing effort to characterize NDDs genetically, we encountered a consanguineous Saudi family where the 14-year-old index individual has early onset global developmental delay (Fig. 1a and d). She was noted in infancy to have an increased head circumference and brain computed tomography (CT) at one year of age showed static hydrocephalus, cerebral cortex atrophy and diminished white matter (Fig. 1f and g and Table 1). The patient was under regular follow-up for increased intracranial pressure (ICP) and a shunt was considered but not performed because it was static. There were no additional signs of increase in ICP, no headaches, and no complaints during her follow-up. Currently, she has intellectual disability, verbalizes single words only, walks unsteadily and has no sphincter control. Her eye examination is significant for high myopia, oculomotor apraxia, microcornea, and nystagmus (Table 1). She has scoliosis, and generalized skin and joint laxity, in addition to generalized hypotonia and muscle weakness. The family was recruited with informed consent under an IRB-approved research protocol (KFSRHC RAC# 2121053). After excluding major chromosomal aberrations by chromosomal

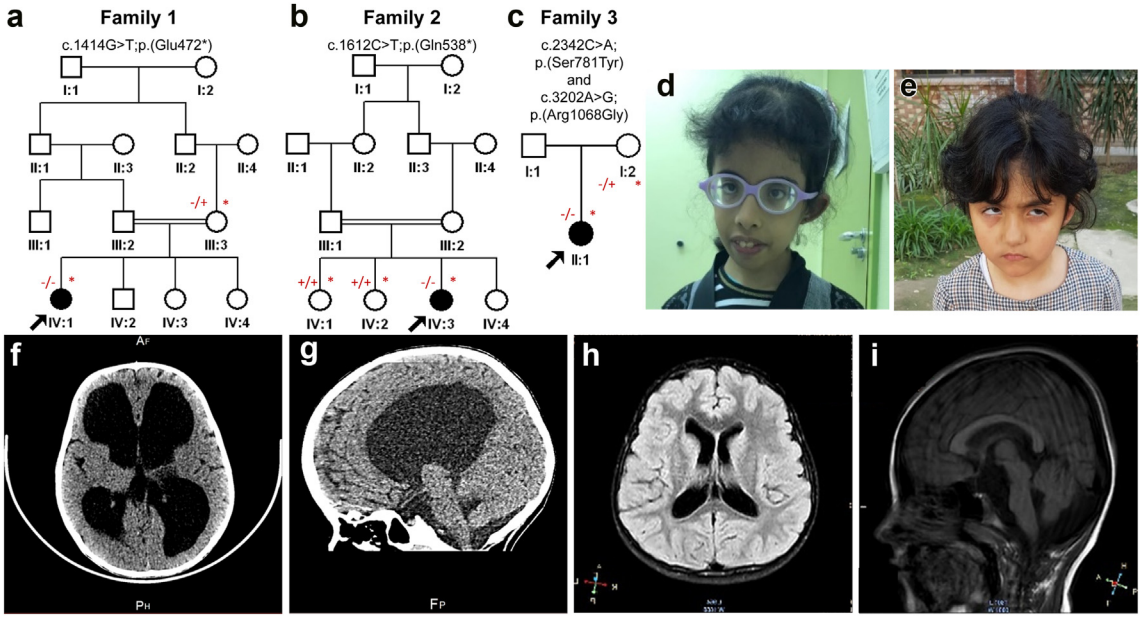


***Fig. 1:* Pedigrees and clinical data of index individuals included in this study.** (a–c) Pedigrees of the three study families with * indicating individuals available for testing. (d and e) Frontal photos of the index individuals from Family 1 and Family 2, respectively illustrating subtle facial dysmorphism in Family 1_IV:1 (elongated face, prominent columella, and overbite). (f and g) Axial and sagittal brain CT cuts for Family 1_IV:1, respectively, depicting abnormally enlarged ventricles (hydrocephalus). (h) An axial brain MRI image for Family 2_ IV:3 showing abnormally dilated ventricles. (i) A sagittal brain MRI image for Family 2_IV:3 showing a cystic area in posterior fossa communicating with the 4th ventricle (Dandy-Walker variant).

microarray,[18] we proceeded with combined exome/autozygome analysis to prioritize ultra-rare homozygous variants within the autozygome as described before.[13] Of the four ultra-rare (MAF <0.001 in gnomAD and a local database of 18,360 exomes), coding/splicing variants, the variant *SLK*: NM_014720.4:c.1414G>T;p.(Glu472*) was noteworthy because it represents a homozygous likely loss-of-function variant in a gene with existing functional impact on dendrite development, at least in the mouse (see above). Indeed, after confirming the presence of this variant in the affected individual's genome using Sanger sequencing as well as confirming its segregation within the family, we performed immunoblot analysis on protein derived from her lymphoblastoid cell line and observed complete absence of full length SLK (Fig. 2d). Importantly, the antibody used (Anti-SLK antibody (ab226986)) targets the N-terminus of the protein and yet no truncated product was visible indicating complete loss of the protein. RT-PCR experiment on RNA from the same lymphoblastoid cell line showed marked reduction of the transcript in comparison to control cell lines suggesting non-sense mediated decay (NMD). The level of NMD was evaluated using quantitative RT-PCR, which revealed 88% reduction of *SLK* levels compared to control (Fig. 2c).

Using GeneMatcher,[19] and our internal database at Lifera Omics of ~70 K genomes and exomes from ethnically matched individuals, we were able to identify three additional affected individuals with a matching phenotype. However, only two agreed to be recruited and are described here. Individual IV:3 from Family 2 is an 8-year-old girl born to a healthy consanguineous couple (first cousins) of Pakistani origin (Fig. 1b and e). Psychomotor delay was evident e.g. head control at 7–8 months, sitting at 8 months, walking at 18 months and verbalizing 2–3 single words at 18 months. Neurological examination revealed generalized hypotonia and muscle weakness as well as bilateral horizontal nystagmus (Table 1). Ophthalmological evaluation revealed macular degeneration (left > right), exotropia and oculogyria. Currently, she functions at a mild intellectual disability level. Brain magnetic resonance imaging (MRI) at the age of 6 years revealed an arachnoid cyst in pre-pontine and interpeduncular cisterns with hydrocephalus and Dandy-Walker variant in the posterior fossa (Fig. 1h and i). After obtaining informed consent, the family was recruited and exome sequencing on the index individual revealed a homozygous truncating variant (*SLK*: NM_014720.4:c.1612C > T; p. (Gln538*)). The premature truncation occurred in the same exon (exon 9 of 19) as the variant we identified in the Saudi family. While no RNA or protein was available for testing, we suspect NMD would function at the same level of efficiency and the transcript expression level would be similarly reduced.

| ID | Family 1_IV:1 | Family 2_IV:3 | Family 3_II:1 |
|---|---|---|---|
| **Variant (NM_014720.4)** | c.1414G > T; p. (Glu472*) | c.1612C > T; p. (Gln538*) | c.2342C > A; p. (Ser781Tyr) & c.3202 A > G; p. (Arg1068Gly) |
| **Type of variant** | Stopgain | Stopgain | Missense |
| **Zygosity** | Homozygous | Homozygous | Compound heterozygous |
| **Gender** | Female | Female | Female |
| **Age** | 14 Years | 8 Years | 19 Years |
| **Ethnicity** | Arab | Pakistani | Greek/English/Hispanic (Cuban) |
| **Growth parameters** | | | |
| At age | 9 years old | 6 years old | 7 years old |
| Weight (kg) | 18 kg, <1 percentile (−2.76 SD) | 21 kg, 42nd percentile (−0.19 SD) | 26.5 kg, 75th percentile |
| Length (cm) | 111 cm, <1 percentile (−3.66 SD) | 117 cm, 42nd percentile (−0.21 SD) | 123 cm, 60th percentile |
| Head circumference (cm) | 55 cm, 99th percentile (+2.32 SD) | 50 cm, 26th percentile | 54 cm, 99th percentile |
| **Development** | | | |
| Failure to thrive | Yes | No | No |
| Gross motor delay | Yes | Yes | No |
| Fine motor delay | Yes | Yes | No |
| Speech delay | Yes | Yes | Yes |
| Intellectual disability | Yes | Yes | Yes |
| **Macrocephaly** | Yes, 99th percentile (+2.32 SD) | No, 26th percentile | Yes, 99th percentile |
| **Dysmorphism** | Subtle | No | Yes |
| **Neurological** | | | |
| Hypotonia | Yes | Yes | Yes |
| Muscle weakness | Yes | Yes | No |
| **Skeletal** | | | |
| Scoliosis | Yes | No | Yes |
| Joint hyperextensibility | Yes | No | Yes |
| **Cutis laxa** | Yes | No | No |
| **Ocular** | | | |
| Oculomotor apraxia | Yes | No | No |
| Strabismus | Yes | Yes | No |
| Oculogyric crisis | No | Yes | No |
| **Other ocular abnormalities** | High myopia, microcornea, nystagmus, poor vision, and difficulty following objects | Bilateral macular degeneration (left > right), apraxia, and poor vision | Rapid eye movements when she reads |
| **Brain MRI/CT** | | | |
| Hydrocephalus | Yes | Yes | No |
| Ventriculomegaly | Yes | Yes | No |
| Cerebral cortex | Atrophy | Unremarkable | Unremarkable |
| White matter | Diminished | Unremarkable | Unremarkable |
| **Other CNS findings** | NA | Arachnoid cyst in pre-pontine and interpeduncular cisterns with obstructive hydrocephalus and Dandy-Walker variant in posterior fossa | None |
| **Other features** | Transient neonatal jaundice, no control over sphincters, and recurrent respiratory infection | Hearing loss and recurrent respiratory infection | Simplified ear helices bilaterally, high arched palate, midface hypoplasia, retrognathia, single palmar crease on right hand, arachnodactyly, and cafe au lait macules. She also has autism, seizures and ADHD |

*Table 1:* **Summary of the clinical features of the three individuals included in this study.**

The other affected individual who agreed to be recruited is individual II: 1 from Family 3, a 19 year old female with past medical history of developmental delay, autism, ADHD, and scoliosis (Fig. 1c, Table 1). She presented with sensory sensitivity to loud noises and repetitive behaviours. She had a history of joint hypermobility and two shoulder dislocations. Her education placement was in a learning disability classroom. Since age 14 years, she started having seizures, many associated with her menstrual period, and her antiepileptic medications altered her stimulatory behaviours and made her regress, before achieving control with lamotrigine 250 mg daily and lacosamide 150 mg bid. The patient developed the first grand mal seizure at age 15. She was started on brivaracetam and experienced regression with behaviour worsening and abnormal

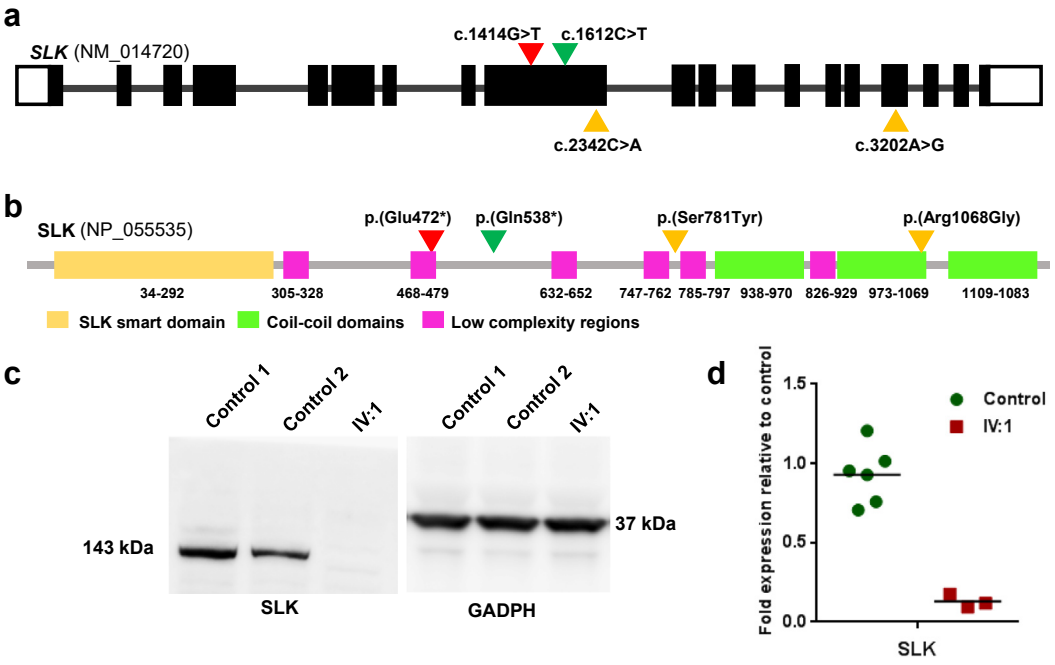


***Fig. 2:*** **Molecular characterization of NDD-associated *SLK* variants.** (a) A schematic representation of the *SLK* gene; the red arrow indicates the variant identified in Family 1 while the green arrow indicates the variant identified in Family 2; both of which map to the same exon (exon 9). The yellow arrows indicate the compound heterozygous missense variants identified in the proband from Family 3 (b) A diagram depicting domains of the SLK protein and locations of identified variants. (c) Representative immunoblot analysis from three different replicates using protein derived from individual from family 1 (IV:1) lymphoblastoid cell line showing complete absence of both the full length as well as the predicted truncated version of the SLK protein. (d) A dot blot chart of qRT-PCR results showing marked reduction in the expression of *SLK* transcript in the index of family 1 (IV:1). The green circle points represent data points collected from three replicates from two different control samples, the red squares represent datapoints collected from three different replicates from the patient sample (IV:1). The horizontal line represents the mean.

movements. Seizures continued and she was started on lamotrigine but developed side effects, so the dose was reduced and clobazam was started. A pattern was observed associated with seizures triggered by her menstrual periods, so acetazolamide was added to clobazam and lamotrigine. Clobazam was stopped and lacosamide was added to lamotrigine and acetazolamide. Once the clobazam was stopped the regression improved back to baseline. Currently, she is on lacosamide, lamotrigine and acetazolamide regimen to this day and has not had a seizure. She had a total of 16 seizures in her life. She has rapid eye movements when she reads. She is unable to have a conversation. She has intact gross and fine motor skills but has a history of hypotonia. She had one episode of fainting at age 13 years old but cardiac workup was normal. Her scoliosis of 28° deviation has not required bracing or surgery. She was born at 39 weeks via C/S for breech position. No NICU stay. Her first words were at 15 months, with some regression at 2 years of age. Family history was negative for developmental delay or learning difficulties. Physical exam findings included simplified ear helices bilaterally, high arched palate, midface hypoplasia, retrognathia, Beighton hypermobility score 9/9, scoliosis, single palmar crease on right hand, arachnodactyly, and cafe au lait macules. Brain MRI showed no evidence of a structural abnormality or acute intracranial findings. Genetic testing was negative for Fragile X, chromosomal microarray and *PTEN* sequencing. Exome sequencing identified two heterozygous variants in the *SLK* gene (NM_014720.4:c.2342C > A; p. (Ser781Tyr) not inherited from her mother and maternally inherited c.3202 A > G; p. (Arg1068Gly)). Table S1 summarizes the frequencies and in silico predictions for the identified variants.

### *SLK* deficiency impairs cell migration and proper cytoskeletal organization

Given the truncating nature of the variants we identified in two of the three individuals with a tentative *SLK*-related NDD, we set out to test if *SLK* deficiency is functionally consequential to the cytoskeletal organization. It has been shown that *SLK* is required for microtubule-dependent focal adhesion turnover and cell migration.[8] Using fibroblasts derived from a skin biopsy taken from individual IV:1 (index individual in family

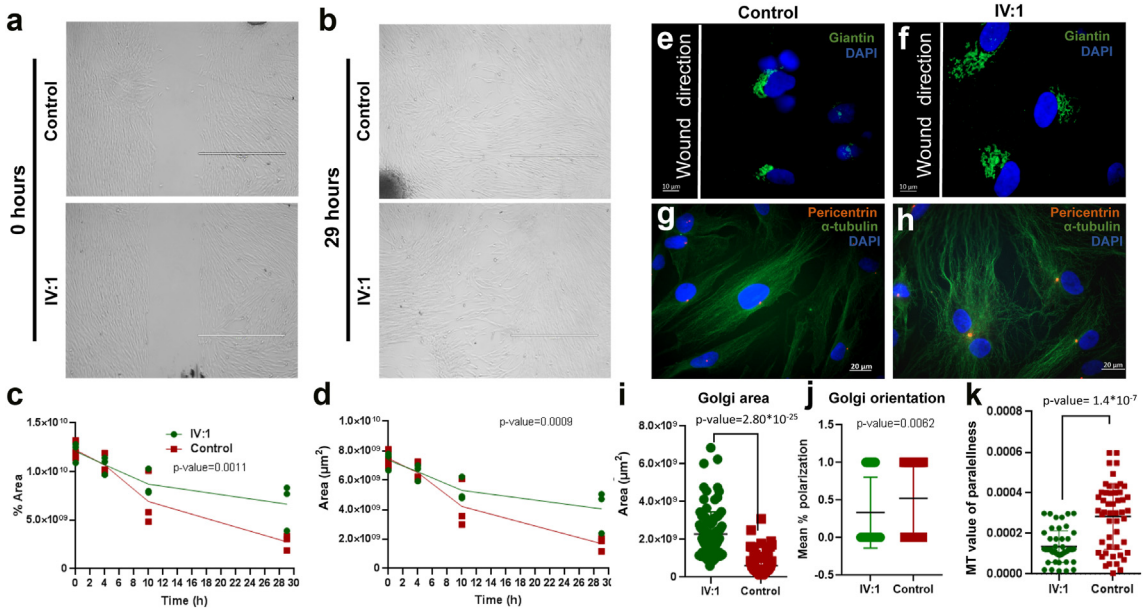


***Fig. 3:*** **Quantification of wound assay, Golgi appearance and microtubule distribution in patient-derived fibroblasts compared to control**. (a) Representative images of sub-confluent fibroblast cells derived from either the index individual in Family 1 (IV:1) or control cell lines at 0 h of wound-induced cell migration assay. Scale bar: 1000 μm. (b) Wound closure was followed serially for 29 h during which a significant difference in cell migration was observed between the two cell lines. Scale bar: 1000 μm. (c) Percent wound closure was evaluated up to 29 h. (d) The remaining area of the wound was measured in $\mu m^2$. The percent wound closure and area of the wound were measured using the ImageJ plugin Wound healing size tool image tool analysis (https://github.com/AlejandraArnedo/Wound-healing-size-tool/wiki).[15] Data from 50 cells were collected and analysed. (e) Control cells showing perinuclear compact and polarized Golgi apparatus that are directed toward the migrating wound edge. (f) IV:1-derived fibroblast cells depicting a dispersed and non-polarized (oriented) Golgi apparatus towards the migrating/wound edge. (g) A representative image of normally polarized and parallel orientated microtubules in control cells. (h) A representative image of individual IV:1-derived fibroblast cells showing an un-polarized chaotic microtubule distribution; microtubules labelled with α-tubulin (green) and the centrosome is labelled with Pericentrin (orange) antibodies. (i) The total area of Golgi from 100 cells was measured using the ImageJ software. Error bars represent stdev. (j) The directional orientation of Golgi from 100 cells was assessed and presented as percent mean polarization with error bars representing stdev of 3 replicates. (k) The direction of orientation (paralellness) of microtubules was measured using the LPX ImageJ plugin (https://lpixel.net/services/research/lpixel-imagej-plugins/)[16]; and data presented as mean and stdev of images of 100 cells. Data from 50 cells were collected and analysed and p-value was calculated based on Welch's t-test for (c, d, i, j and k). The red squares represent datapoints collected from control sample, the green circles represent datapoints collected from the patient sample (IV:1). The horizontal line represents the mean.

1), we performed a standard wound assay as described before.[8,20] As previously noted by Burakov and colleagues, we observed significant impairment of cell migration (Fig. 3a–d). We were also able to recapitulate the results using shRNA knockdown of *SLK* (Fig. S1a). Similarly, we were able to replicate the previously reported impact of *SLK* deficiency on Golgi appearance in migrating cells.[20] Unlike their compact and polarized appearance in control cells, Golgi appeared significantly more dispersed and non-polarized (oriented) towards the migrating/wound edge (Fig. 3e, f, i, and j). Finally, we set out to test the effect of *SLK* deficiency on the organization of the cytoskeleton, which was reported to display a chaotic appearance.[20–22] Unlike the organized parallel orientation of microtubules in control cells, they appeared significantly irregular and chaotic in cells derived from the affected individual (Fig. 3g, h, and k). Taken together, our results suggest that the loss-of-function variant we observed in individual IV:1, and potentially by extension the other likely loss -of-function variants, are likely null and the resulting severe *SLK* deficiency may result in major cytoskeletal defects similar to those observed under induced deficiency states.

### Human SLK-deficient fibroblasts exhibit distinct compositions in focal adhesions (FAs)

The impact of *SLK* gene deficiency on the composition of FAs in human fibroblasts was investigated through the isolation of FA proteins from both wild-type and SLK-deficient cells. Utilizing LC-MS/MS analysis, we discerned distinctive compositions within FAs. Our mass spectrometry data revealed the presence of essential components necessary for FA assembly in both cell lines, such as Integrin αvβ3, Integrin α5β1, Talin1, Ras-related protein Rap1b, Vinculin, KANK2, Kindlin-2,

Zyxin, VASP, alpha-actin 1, and actin (refer to Table S2). RIAM was not detected in both cell lines, suggesting the isolation of mature FAs rather than nascent adhesions enriched with RIAM. Further analysis uncovered differences in the Integrin category within SLK-deficient fibroblasts. Whereas both Integrin αvβ3 and Integrin α5β1 were present, SLK-deficient samples exhibited distinct Integrin alpha categories (Integrin alpha 1, 8) compared to wild-type samples (Integrin alpha 1, 2, 3, 4, 11) (see Supplementary Files 1–6). FAK was not detected in SLK-deficient samples, suggesting a potential weakening of the connection between FAK and its binding partners within FAs. Additionally, Paxillin and Talin-2 were not detected in the isolated adhesion samples from SLK-deficient fibroblasts. This discrepancy suggests that SLK deficiency may disrupt the normal association of Paxillin and Talin-2 with their ligands within FAs (refer to Table S2).

To investigate the influence of SLK on Paxillin localization, we conducted immunofluorescence experiments using Vinculin as a FA marker. The observations revealed colocalization of Paxillin and Vinculin in both cell lines, suggesting that the absence of SLK does not alter Paxillin's positioning within FAs. However, SLK-deficient fibroblasts exhibited a more rounded cell morphology compared to the wild-type, lacking the obvious fibrillar structures characteristic of polarized fibroblasts. The absence of fibrillar adhesions (axial ratio >7[23]), which is a pre-signal of fibroblast polarization,[24] indicates compromised tension or contractility generation in SLK-deficient cells. This deficiency may contribute to the observed round cell morphology and the difficulty of SLK-deficient cells to detach. These results align with the expectations from Quizi et al.,[7] where serine 250 phosphorylation is implicated in paxillin redistribution and cell motility. However, our study reveals this effect through the SLK deficiency, rather than by a paxillin mutation that impairs its phosphorylation.

To further investigate the effects of SLK on Paxillin localization at adhesion sites and cell morphology, SLK expression was reduced in wild-type (WT) fibroblasts via gene silencing. Immunofluorescence staining showed that Vinculin colocalizes with Paxillin at adhesion sites in both SLK-silenced and WT cells, suggesting that Paxillin positioning at adhesions is independent of reduced SLK expression. Additionally, in the three SLK-silenced samples, some cells formed prominent fibrillar adhesions similar to WT cells. However, cells with strong GFP signals from SLK-shRNA lentiviral particles displayed fewer fibrillar adhesions, instead showing more dot-like adhesions, as seen in rows 2 and 3 of shRNA A and shRNA B in Fig. 1. These findings suggest that decreased SLK expression impairs the maturation of adhesions, consistent with previous observations in SLK-deficient cells. Moreover, these SLK-silenced cells exhibited diverse morphologies, contrasting with the typical round shape of SLK-deficient cells. This morphological variation is likely due to incomplete SLK silencing.

Taken together, our investigation suggests that SLK-deficient fibroblasts display different Integrin categories in FAs compared to wild-type cells and that SLK deficiency may disrupt the association of FAK, Talin-2, and Paxillin with other FA components, without affecting Paxillin's positioning within FAs. Particularly striking is the direct association between SLK and cell polarization. These findings provide valuable insights into the nuanced role of SLK in the molecular composition and organization of FAs in human fibroblasts.

### Transdifferentiated neurons from patient fibroblasts display abnormal morphology

To elucidate the morphological changes associated with *SLK*-mutated neurons, we transdifferentiated fibroblasts into neurons. We first confirmed that the fibroblasts from control patients had normal levels of SLK, while those isolated from the *SLK* mutant patients lacked *SLK* expression (Fig. 4b and c and Fig. S1b and c). We then transdifferentiated these fibroblasts into neurons using a lentiviral vector encoding for Ascl1 and Brn2 (Fig. 4d) (See methods for more details). After 12 days of viral transduction, the cells acquired neuronal like morphologies and were found to be positive for NeuN, a pan neuronal marker, beta-tubulin III and Map2 (neurite markers) (Fig. 4d bottom panel). The transdifferentiated neurons derived from control subjects displayed normal neuronal morphologies and arborizations and displayed normal tiling of the neurons in the dish. On the other hand, while the neurons derived from SLK-deficient cells had normal cell body diameter and neurite length (Fig. 4eii, iv), morphological analysis of the transdifferentiated cells revealed that SLK mutant fibroblasts formed larger cell clusters compared to control fibroblasts, suggesting altered cell–cell adhesion or proliferation during differentiation (20.73 ± 7.19 control vs 258.3 ± 26.35 um in SLK deficient fibroblasts, $p = 0.0256$ (Mann Whitney test) Fig. 4d and e-i) Immunostaining of the transdifferentiated fibroblasts with Tubulin. β-III and Map2, markers of neuronal differentiation, showed fewer and shorter neurites in *SLK* knockdown cells and SLK patient derived fibroblasts compared to controls, suggesting that *SLK* knockdown impairs the proper maturation of neuronal morphology (Fig. 4eiii).

To independently confirm that there are morphological changes associated with SLK-deficient neurons, we performed shRNA mediated knockdown of SLK in control fibroblasts. We first analysed the differences in the SLK expression in the shRNA mediated knockdown of SLK in control fibroblasts (Fig. 4f and g, Fig. S1b and c). First, we confirmed that the shRNA mediated knockdown strategy resulted in a significant reduction

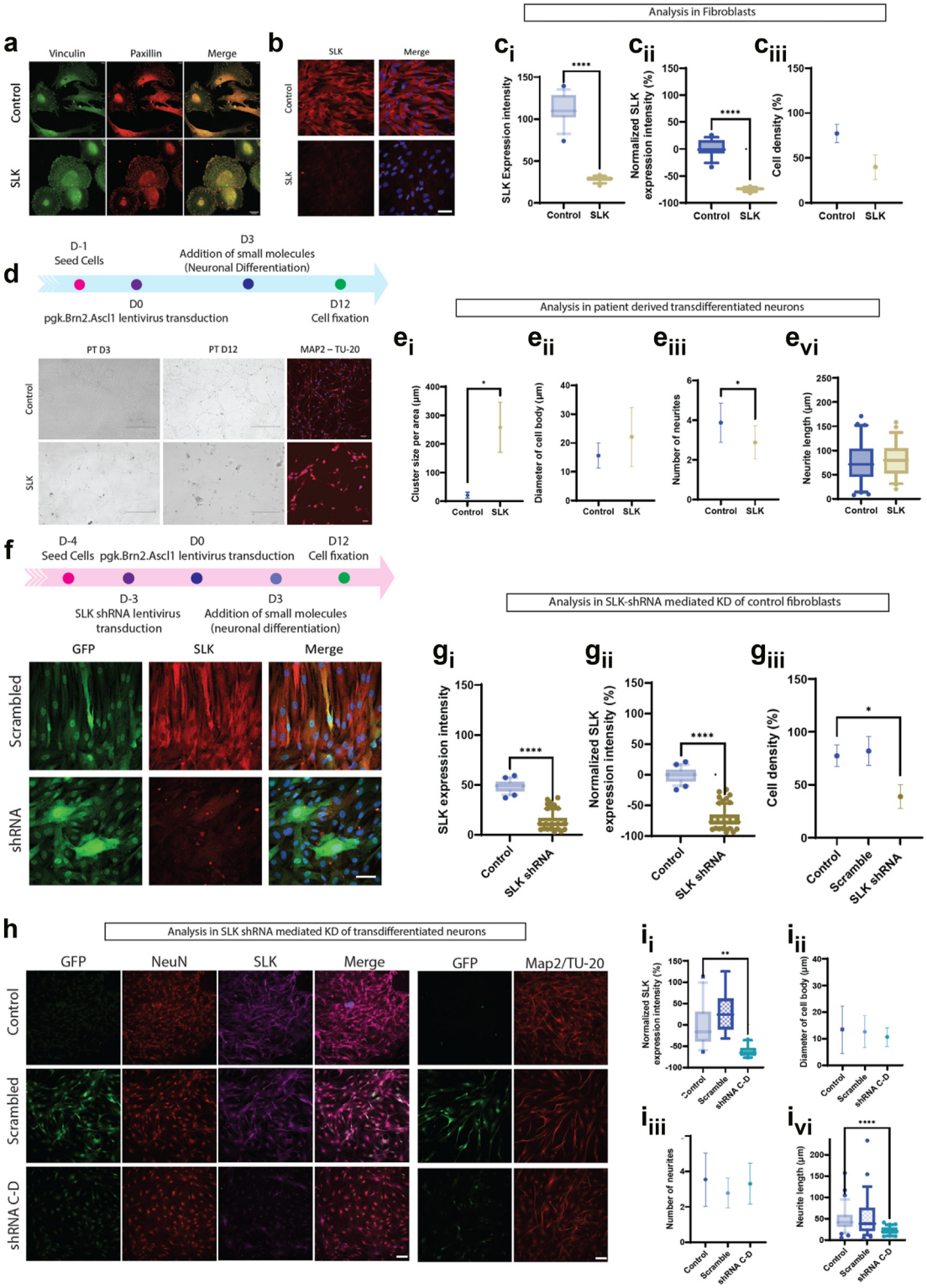


***Fig. 4*: The effect of *SLK* deficiency on Paxillin localization and neuronal differentiation**. (a) Immunofluorescence staining for Paxillin and Vinculin in fibroblasts derived from the index individual in Family 1 (IV:1) (SLK) and control (Control/WT) cell lines. Green and red represent Vinculin and Paxillin, respectively, while yellow indicates their colocalization. The scale bar in the bottom right corner denotes a length of

in SLK expression compared to control fibroblasts, indicating successful knockdown (KD) of SLK. We tested 4 different shRNAs against SLK, and 2 scrambled shRNAs as controls. Individual shRNAs yielded on average a 60% decrease in SLK expression (Fig. S1f–i), however a combination of two shRNAs together resulted in a larger decrease. Quantitative analysis revealed that SLK expression in the knockdown fibroblasts (SLK KD) was significantly lower than in controls (control-0.00001 ± 2.7% vs SLK shRNA KD −72.11 ± 15.8% decrease, $p < 0.001$ (Mann–Whitney test); Fig. 4f lower panel and Fig. 4h and i, Fig. S1b–f), confirming the efficiency of the knockdown. In addition, we noted a modest but significant decrease in cell density in the SLK knockdown cells compared to controls ($p = 0.0179$ (Kruskal–Wallis test); Fig. 4g-iii and Fig. S1d-ii), suggesting that like fibroblasts derived from SLK mutated patients, SLK KD fibroblasts undergo a slower process of proliferation. We next investigated the effect of SLK knockdown on neurons by transdifferentiating the SLK KD fibroblasts into neurons like before (Fig. 4f upper panel). We transdifferentiated fibroblasts into neurons using a lentiviral vector encoding for Ascl1 and Brn2 in either control or in shRNA mediated knockdown of control fibroblasts (See methods for more details). After 12 days of viral transduction, the cells acquired neuronal like morphologies and were found to be positive for NeuN, a pan neuronal marker, beta-tubulin III and Map2 (neurite markers) (Fig. 4h). Morphological analysis of the transdifferentiated neurons of the SLK KD fibroblasts revealed that there is a decrease in the neurite length but not in number of neurites. While these changes did not fully recapitulate the phenotype observed in patient derived fibroblasts, they did cause an impairment in morphological maturation, suggesting that SLK is required for the establishment of proper neuronal morphologies.

Together, these findings suggest that SLK plays a critical role in the regulation of neuronal differentiation, impacting cell morphology. The significant reductions in neurite formation and altered cell morphology in *SLK* knockdown cells highlight the potential importance of SLK in maintaining proper cellular architecture of neurons.

### Neuron-specific silencing of *Slik*, *Drosophila* homologue of human *SLK*, induced neuromuscular developmental defects

SLK is highly conserved across different species from flies to humans. In drosophila, *Slik* is the only predicted orthologue of human *SLK*. *Slik* encodes a kinase that has a highly conserved Serine/threonine-protein kinase domain at the N-terminus (Fig. S2). *Slik* is expressed in most cell types, with a high expression level in CNS (Fig. S3). To further investigate the roles of *Slik* in neuronal development, we knocked down the expression of *Slik* specifically in the nervous system using the neuron-specific driver elav-Gal4, combined with RNAi knockdown of *Slik* (UAS-*Slik*-RNAi). Two independent RNAi lines were tested, which provided the same results (representative data for one UAS-*Slik*-RNAi line (BDSC ID: 55626) are shown in Fig. 5).

The 3rd instar larval brain, ventral ganglion (Fig. 5a) was stained with HRP to visualize its structure (Fig. 5b). Compared to control larvae, silencing *Slik* significantly increased the size of the ventral ganglion, resulting in a macrocephaly phenotype (Fig. 5c). Next, we examined the synaptic changes at the neuromuscular junction (NMJ) caused by neuron-specific silencing of *Slik*. *Drosophila* NMJ was a well-characterized model of synapse function, offering crucial insights into synaptic transmission, plasticity, and regeneration, which are the key aspects of human CNS function and pathology.[25,26] NMJ was stained with HRP to visualize its structure

20 μm. (b) Anti-SLK immunostaining on control and SLK mutant patient fibroblasts, scale bar = 50 μM. (**$c_i$**) SLK expression intensity in control vs SLK mutant fibroblasts ($p < 0.0001$ (unpaired t-test with Welch's correction)). ($c_{ii}$) Normalized SLK expression percentage in control vs SLK mutant fibroblasts ($p < 0.0001$ (unpaired t-test with Welch's correction)). ($c_{iii}$) Percentage change in cell density between control and SLK mutant fibroblasts (Kruskal–Wallis test, $p = 0.1039$). (d) Schematic representation of the transdifferentiation protocol (top panel). Representative images of control and SLK patient derived fibroblasts (PT D3 refers to 3 days post transduction with Brn2 and Ascl1 lentivirus, scale bar = 300 μM), transdifferentiated neurons (PT D12, 12 days after transduction; scale bar = 300 μM) and transdifferentiated fibroblasts were stained with Tubulin β-III and Map2. Scale bar = 50 μM. ($e_i$) Statistical analysis of the transdifferentiated SLK patient derived fibroblasts. ($p = 0.0256$ (Mann Whitney test of normalized cluster size)) and cell body diameter ($e_{ii}$, $p = 0.1229$ (Unpaired t-test with Welch's correction of the number of neurites)). ($e_{iii}$, $p = 0.0471$(Unpaired t-test with Welch's correction of the number of neurites)) and length of neurites ($e_{iv}$, $p = 0.7643$ (Unpaired t-test with Welch's correction of the number of neurites)). (f) Schematic representation of lentiviral shRNA mediated knockdown (KD) of SLK followed by transdifferentiation to produce neurons (upper panel). shRNA mediated knockdown (KD) of SLK derived fibroblasts indicating the efficiency of the KD (bottom panel, Scale bar = 50 μM). ($g_i$) Analysis in fibroblasts reveals that the shRNA mediated KD of SLK resulted in a marked reduction in SLK expression intensity ($p < 0.0001$ (Mann–Whiteny test)). (**$g_{ii}$**) Normalized SLK expression percentage decrease (Control vs shRNA mediated KD of SLK fibroblasts, ($p < 0.0001$ (Mann–Whiteny test)). ($g_{iii}$) Percentage change in cell density between control, scrambled shRNA and shRNA mediated KD of SLK fibroblasts ($p = 0.0179$ (Kruskal–Wallis test)). (h) Representative images of control, scrambled shRNA and shRNA mediated KD of SLK transdifferentiated neurons at 20× magnification. Scale bar = 300 μM. Please note the reduction in the SLK intensity in neurons derived from shRNA KD fibroblasts. ($i_i$) Normalized percentage change in SLK expression intensity (Control vs scrambled shRNA vs shRNA mediated KD of SLK fibroblasts, $p = 0.0089$ (Brown-Forsythe and Welch ANOVA tests) and (**$i_{ii}$**, $p = 0.1773$ (Kruskal–Wallis test, of the diameter of cell body)), number of neurites ($I_{iii}$, $p = 0.0178$ (Kruskal–Wallis test, of the diameter of cell body)) and neurite length ($I_{iv}$, $p < 0.0001$ (Kruskal–Wallis test, of the diameter of cell body)).

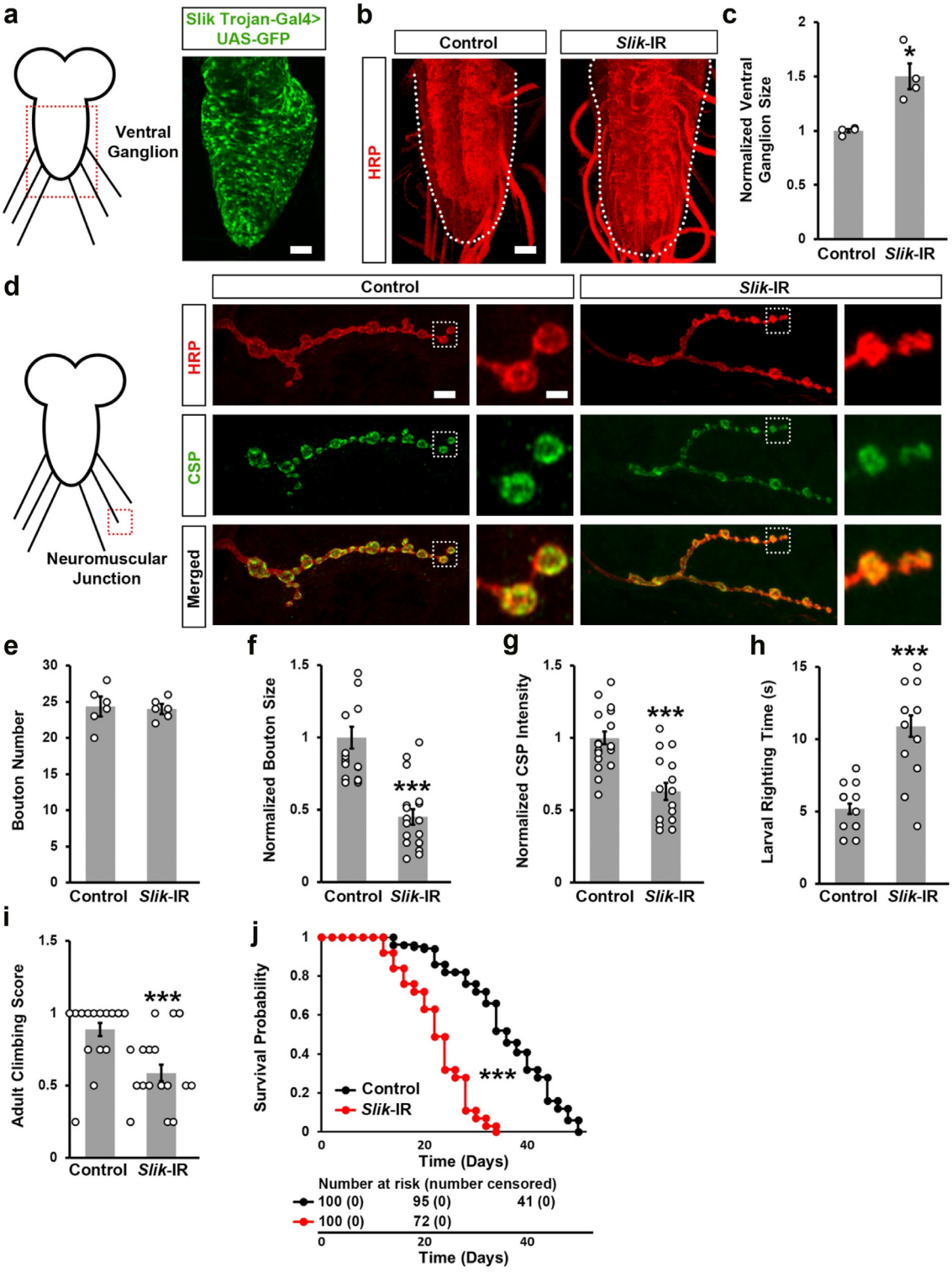


***Fig. 5:* Neuromuscular appearance and function in *Drosophila* larvae with silenced Slik compared to control.** (a) On the left, a graphic representation of the *Drosophila* larval central nervous system. Red dotted lines delineate the outline of the ventral ganglion. On the right, the *Drosophila* larval ventral ganglion was visualized by GFP (green fluorescence) induced by *Slik* Trojan-Gal4. Scale bar: 40 μm. (b) *Drosophila* larval

(Fig. 5d). Compared to control larvae, silencing *Slik* did not change the number of boutons (Fig. 5e), but it did significantly reduce bouton size (Fig. 5f), which affects synapse maturation. To further investigate the developmental changes in response to *Slik* silencing, we checked the level of the synaptic vesicle Cysteine-string protein (CSP) (Fig. 5d). Compared to control larvae, silencing *Slik* significantly reduced the CSP level (Fig. 5g). These results indicate that silencing *Slik* leads to developmental defects of the NMJ. These NMJ defects caused a locomotion defect observed in both early in larvae and later in the adult flies (Fig. 5h and i). Moreover, the adult flies that emerged showed markedly shortened lifespans compared to control flies (Fig. 5j). For the control group, all flies reached their lifespan endpoint at 50 days old, while the *Slik*-IR flies died at 34 days old. The interquartile range (IQR) for the control group is Q1 is 30 days, Q2 is 34 days and Q3 is 44 days, while the IQR for *Slik*-IR flies is 18, 22, and 26 days.

### Neuromuscular developmental defects induced by *Drosophila Slik* silencing can be rescued by introducing wildtype but not mutant human *SLK*

Next, we wanted to demonstrate functional conservation between *Drosophila Slik* and human *SLK* and identify the approach which can be used to validate the disease variants identified in the patients. Neuron-specific expression of wildtype human *SLK* in the *Slik* silencing flies, completely restored the neuromuscular developmental defects, including the enlarged nervous system phenotype, NMJ bouton size reduction, CSP level reduction in presynapses, and locomotion defects in both larvae and adult flies (Fig. 6a–g).

To functionally validate the *SLK* variants identified in the human patients, we performed rescue experiments in *Drosophila*. We found that *Drosophila Slik* silencing induced neuromuscular developmental defects and wildtype human *SLK* can rescue this phenotype. Here, we expressed human *SLK* carrying a patient variant and assessed its ability to rescue the neuromuscular developmental defects induced by *Drosophila Slik* silencing.

We observed that none of the *SLK* variants identified in the patients (E472*, Q538*, S781Y and R1037G) can restore the neuromuscular developmental defects, including the enlarged CNS phenotype, NMJ bouton size reduction, CSP level reduction in presynapses, and locomotion defects in both larvae and adult flies (Fig. 6a–g). These findings indicate a loss-of-function mechanism for these variants and provide *in vivo* evidence to confirm their pathogenicity.

## Discussion

Many genes with important roles in the organization of the cytoskeleton have been implicated in neurodevelopmental disorders. Most genes linked to primary microcephaly regulate the orientation of mitosis of neural progenitors. This regulation maintains the delicate balance between symmetric and asymmetric cell division such that pathogenic variants in these genes perturb the balance and cause early depletion of these stem-like cells leading to microcephaly. Many NDDs that lack such major brain malformations as primary microcephaly harbour more subtle structural defects that are only discernible on microscopic examination of the brain. Dendrites and dendritic spines in particular have come under sharper focus thanks to these disorders several of which are caused by genes with cytoskeletal roles.[27] Indeed, the cytoskeletal components of dendritic spines (cortactin, ARP2/3 complex, PSD 95/93, cofilin, actin filaments, and the regulatory Rho GTPases Rac, Rho, and Cdc42) are enriched for genes linked to intellectual disability.[28,29] Of note, several cytoskeletal proteins have been identified as substrates of the kinase activity of SLK including RhoA, ezrin, paxillin, and dynactin, and these have established roles in dendrite development.

We suggest that SLK is another cytoskeletal organizer whose deficiency results in NDD. Until recently, only other members of the Ste20/Hippo kinase family have been shown to control neuronal morphology and synapse formation, such as TAOK1/2, MINK, TNIK, MSN, and MST3b.[30] Investigating a potential neuronal function of *SLK* using mouse knockouts was precluded

macrocephaly phenotype induced by elav-Gal4, neuron-specific expression of UAS-RNAi transgene targeting *Slik*. The *Drosophila* larval ventral ganglion was visualized by HRP (red). Scale bar: 40 μm. (c) Quantitation of *Drosophila* larval ventral ganglion size relative to that in control larvae. N = 6 larvae per genotype. (d) On the left, a graphic representation of the *Drosophila* larval central nervous system. Red dotted lines delineate the outline of the neuromuscular junction (NMJ). On the right, *Drosophila* larval NMJ phenotype induced by elav-Gal4, which drives neuron-specific expression of a UAS-RNAi transgene targeting Slik. The *Drosophila* larval NMJ was visualized by HRP (red). Synaptic vesicle protein CSP was detected by immunofluorescence (green). Scale bar: 10 μm. Scale bar magnification: 2 μm. (e and f) Quantitation of *Drosophila* larval NMJ bouton number and size compared to that in control larvae. N = 6 larvae per genotype. (g) Quantitation of *Drosophila* larval NMJ CSP intensity relative to that in control flies. N = 6 larvae per genotype. (h) Quantitation of *Drosophila* larval righting time. N = 20 larvae per genotype. (i) Quantitation of climbing ability in adult flies. N = 40 flies per genotype. (j) Survival curves for adult flies expressing *Slik* RNAi transgenes in their nervous system. N = 100 flies per genotype. Results have been presented as mean ± s.e.m., normalized to the control group. Statistical significance was defined as *p < 0.05, **p < 0.01, ***p < 0.001 (Student's t-test for normal distributed data or Mann–Whitney test for nonnormal distributed data).

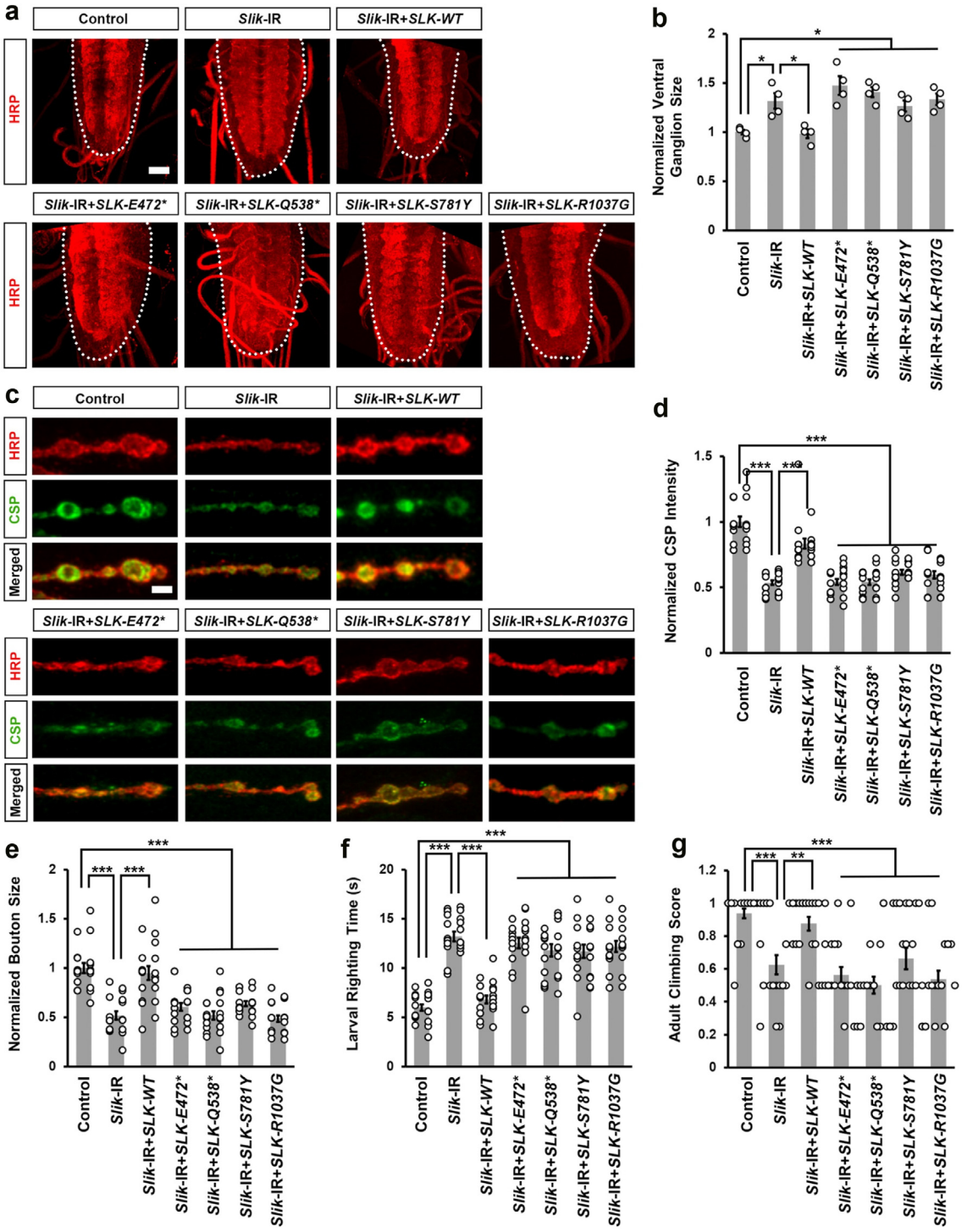


*Fig. 6:* **Neuromuscular developmental defects induced by *Drosophila Slik* silencing can be rescued by wildtype human *SLK*, but not NDD-associated variants**. (a) *Drosophila* larval macrocephaly phenotype induced by elav-Gal4, neuron-specific expression of UAS-RNAi transgene targeting *Slik*. This macrocephaly phenotype can be restored by wildtype human SLK, but not disease variants. The *Drosophila* larval ventral ganglion was visualized by HRP (red). Scale bar: 40 μm. (b) Quantitation of *Drosophila* larval ventral ganglion size relative to that in control larvae. N = 6 larvae per genotype. (c) *Drosophila* larval NMJ phenotype induced by elav-Gal4, which drives neuron-specific

by their embryonic lethality.[31] Therefore, Schoch et al. recently used intraventricular intrauterine electroporation (IUE) of shRNA to achieve *Slk* knockdown in developing cortical neurons. They first established that higher order (beyond 1st and 2nd) dendrites were reduced by >40% in knockdown experiments using primary cortical neurons suggesting a selective role of *SLK* in the development of the distal dendritic tree. A similar pattern was subsequently observed in electroporated developing (E14) cortical neurons that displayed marked reduction (>60%) of higher order dendrites. This effect was lacking, however, when adult (P30–P32) animals were electroporated. To explore the mechanistic basis, they investigated the localization of SLK in neurons and found strong colocalization with phalloidin in the growth cones and tips of neurites, and with MAP-2 in the cell body. They additionally observed a much stronger colocalization with gephyrin puncta than PSD95 puncta on dendritic shafts, which suggests a selective presence of SLK at inhibitory synapses. This was corroborated by finding a marked reduction in inhibitory synapse density, and an accompanying pronounced loss of functional inhibitory input. Interestingly, *SLK* expression was reduced in focal cortical malformations but not the adjacent brain tissue.[12]

We suggest that, similar to the marked disruption of cytoskeletal homoeostasis observed in their fibroblasts, the affected individuals lack *SLK* modulation of cytoskeletal dynamics, a prerequisite for normal dendrite branching.[32,33] Indeed, transdifferentiated neurons from patients with complete SLK-deficiency displayed a marked reduction in the dendrites (neurite numbers) which suggests that similar to the mouse model, human derived neurons display a similar phenotype. By extrapolating from the murine model, it is likely that the neurodevelopmental phenotype we observe in our cohort is the clinical consequence of failure to form higher order dendrites because the length and structure of the dendritic arbour correlates strongly with brain function. It is also likely that lack of *SLK* impaired the interaction of inhibitory synapse-specific protein scaffold with actin, microtubules, and interacting proteins leading to reduced density of inhibitory synapses. This impaired balance of excitatory and inhibitory inputs is known to cause a range of neurodevelopmental phenotypes including intellectual disability as seen in this cohort.

Previous studies have suggested that Paxillin phosphorylation by SLK does not significantly impact Paxillin's localization within FAs, aligning with our immunofluorescence results that show unaffected Paxillin colocalization in the presence of SLK deficiency. However, Quizi et al. have demonstrated the crucial role of SLK-mediated phosphorylation in Paxillin for adhesion turnover and cell migration. In our current investigation, we extend these findings by highlighting that SLK LOF not only affects Paxillin phosphorylation but also impairs cell polarization by inhibiting the assembly of fibrillar adhesions. This observation provides additional insights into the functional consequences of SLK deficiency, emphasizing its impact on both molecular signalling pathways and cellular morphology. Our results, therefore, contribute to a more comprehensive understanding of the intricate relationship between SLK, Paxillin, and FA dynamics.

SLK is highly conserved between human and fly. The Drosophila RNAi Screening Center (DRSC) Integrative Orthologue Prediction Tool (DIOPT; version 8.5), which identifies between species orthologs based on alignment and function, score for human SLK and fly Slik is 11 (out of 15). This provided confidence to use *Drosophila* for functional studies into Slik deficiency-associated phenotypes. In addition to the brain structural and cognitive abnormalities, individuals with *SLK* variants presented with hypotonia and motor delays. Both fly larvae and adults deficient for Silk showed evidence of muscular weakness. Consistently, *Slk* knockout in mouse skeletal muscle has previously been shown to lead to a myopathy and muscle weakness.[34]

In conclusion, we report the first human "knockouts" for *SLK*. The cytoskeletal phenotype observed in cells from affected individuals suggests a similar impact on developing neuronal cytoskeleton, which had been shown experimentally to impair dendrite arborization and the inhibitory/excitatory balance in the brain. Although we cannot exclude the possibility of other variants contributing to the observed phenotype, additional cases will add to our understanding of the genotype-phenotype pattern of this newly identified neurodevelopmental disorder.

expression of a UAS-RNAi transgene targeting Slik. This neuronal defect can be restored by wildtype human *SLK*, but not disease variants. The *Drosophila* larval NMJ was visualized by HRP (red). Synaptic vesicle protein CSP was detected by immunofluorescence (green). Scale bar: 2 μm. (d) Quantitation of *Drosophila* larval NMJ CSP intensity relative to that in control flies. N = 6 larvae per genotype. (e) Quantitation of *Drosophila* larval NMJ bouton size compared to that in control larvae. N = 6 larvae per genotype. (f) Quantitation of *Drosophila* larval righting time. N = 20 larvae per genotype. (g) Quantitation of climbing ability in adult flies. N = 40 flies per genotype. Results have been presented as mean ± s.e.m., normalized to the control group. Statistical significance was defined as $*p < 0.05$, $**p < 0.01$, $***p < 0.001$ (one-way analysis of variance followed by a Tukey–Kramer post-test for normal distributed data or Kruskal–Wallis H-test followed by a Dunn's test for non-normal distributed data).

### Contributors

NA, FSA, ZH, HH and JZ contributed to conception and design of the study. SE, HL, FA, AA, FR, MC, SM, HSA, MH, AA, JAMA, IS, PY, STA, RH, and LI worked on acquisition and analysis of data. FSA, LA, ZH, RM, and JZ helped in draughting a significant portion of the manuscript or figures. List of members of the SYNaPS Study Group is in Supplemental Text. All authors read and approved the final version of the manuscript. LA, FSA, ZH, LI, STA, and HH have accessed and had verified the underlying data. SYNaPS Study Group is an initiative is funded by a Strategic Award from the Wellcome Trust to a team of researchers at the UCL Institute of Neurology and King's College London. Queen Square Genomics provides diagnoses for complex neurological disorders.

### Data sharing statement

Data collected and analysed for this manuscript are available upon request.

### Declaration of interests

FSA is a paid employee of Lifera Omics.

### Acknowledgements

We are grateful to all patients and families whose participation in the study enabled the data collection and the analyses. Family 2 was collected as part of the SYNaPS Study Group collaboration funded by The Wellcome Trust and strategic award (Synaptopathies) funding (WT093205 MA and WT104033AIA). This research was conducted as part of the Queen Square Genomics group at University College London, supported by the National Institute for Health Research University College London Hospitals Biomedical Research Centre. The research was supported by the Bioscience Core Lab, ACL Proteomics Lab and the Imaging and Characterization Core Lab at King Abdullah University of Science & Technology (KAUST) in Thuwal, Saudi Arabia.

Funding: HH is funded by The MRC (MR/S01165X/1, MR/S005021/1, G0601943), The National Institute for Health Research University College London Hospitals Biomedical Research Centre, Rosetree Trust, Ataxia UK, MSA Trust, Brain Research UK, Sparks GOSH Charity, Muscular Dystrophy UK (MDUK), Muscular Dystrophy Association (MDA USA). SE is supported by an MRC strategic award to establish an International Centre for Genomic Medicine in Neuromuscular Diseases (ICGNMD) MR/S005021/1. Z.H. is supported by the National Institutes of Health (NIH) grants HL134940 and DK098410. The research by IS, PY, NLA, LI and STA reported in this publication was supported by King Abdullah University of Science and Technology (KAUST) through the baseline fund to STA and LI as well as to STA and LI, and the KAUST Center of Excellence for Smart Health (KCSH), under award number 5932.

### Appendix A. Supplementary data

Supplementary data related to this article can be found at https://doi.org/10.1016/j.ebiom.2025.105725.

### References

1 Ferrante M, Migliore M, Ascoli GA. Functional impact of dendritic branch-point morphology. *J Neurosci*. 2013;33(5):2156–2165.
2 Scott EK, Luo L. How do dendrites take their shape? *Nat Neurosci*. 2001;4(4):359–365.
3 Kapitein LC, Hoogenraad CC. Building the neuronal microtubule cytoskeleton. *Neuron*. 2015;87(3):492–506.
4 Yadav S, Oses-Prieto JA, Peters CJ, et al. TAOK2 kinase mediates PSD95 stability and dendritic spine maturation through Septin7 phosphorylation. *Neuron*. 2017;93(2):379–393.
5 Wagner S, Flood TA, O'Reilly P, Hume K, Sabourin LA. Association of the Ste20-like kinase (SLK) with the microtubule: role in Rac1-mediated regulation of actin dynamics during cell adhesion and spreading. *J Biol Chem*. 2002;277(40):37685–37692.
6 Sabourin LA, Seale P, Wagner J, Rudnicki MA. Caspase 3 cleavage of the Ste20-related kinase SLK releases and activates an apoptosis-inducing kinase domain and an actin-disassembling region. *Mol Cell Biol*. 2000;20(2):684–696.
7 Quizi JL, Baron K, Al-Zahrani K, et al. SLK-mediated phosphorylation of paxillin is required for focal adhesion turnover and cell migration. *Oncogene*. 2013;32(39):4656–4663.
8 Wagner S, Storbeck CJ, Roovers K, et al. FAK/src-family dependent activation of the Ste20-like kinase SLK is required for microtubule-dependent focal adhesion turnover and cell migration. *PLoS One*. 2008;3(4):e1868.
9 Zhang Y-H, Hume K, Cadonic R, et al. Expression of the Ste20-like kinase SLK during embryonic development and in the murine adult central nervous system. *Brain Res Dev Brain Res*. 2002;139(2):205–215.
10 Sabourin LA, Rudnicki MA. Induction of apoptosis by SLK, a Ste20-related kinase. *Oncogene*. 1999;18(52):7566–7575.
11 Al-Zahrani KN, Sekhon P, Tessier DR, et al. Essential role for the SLK protein kinase in embryogenesis and placental tissue development. *Dev Dyn*. 2014;243(5):640–651.
12 Schoch S, Quatraccioni A, Robens BK, et al. Ste20-like kinase is critical for inhibitory synapse maintenance and its deficiency confers a developmental dendritopathy. *J Neurosci*. 2021;41(39):8111–8125.
13 Monies D, Abouelhoda M, AlSayed M, et al. The landscape of genetic diseases in Saudi Arabia based on the first 1000 diagnostic panels and exomes. *Hum Genet*. 2017;136(8):921–939.
14 Efthymiou S, Salpietro V, Malintan N, et al. Biallelic mutations in neurofascin cause neurodevelopmental impairment and peripheral demyelination. *Brain*. 2019;142(10):2948–2964.
15 Suarez-Arnedo A, Torres Figueroa F, Clavijo C, Arbeláez P, Cruz JC, Muñoz-Camargo C. An image J plugin for the high throughput image analysis of in vitro scratch wound healing assays. *PLoS One*. 2020;15(7):e0232565.
16 Higaki T. Quantitative evaluation of cytoskeletal organizations by microscopic image analysis. *Plant Morphol*. 2017;29(1):15–21.
17 Drouin-Ouellet J, Pircs K, Barker RA, Jakobsson J, Parmar M. Direct neuronal reprogramming for disease modeling studies using patient-derived neurons: what have we learned? *Front Neurosci*. 2017;11:530.
18 Al-Qattan SM, Wakil SM, Anazi S, et al. The clinical utility of molecular karyotyping for neurocognitive phenotypes in a consanguineous population. *Genet Med*. 2015;17(9):719–725.
19 Sobreira N, Schiettecatte F, Valle D, Hamosh A. GeneMatcher: a matching tool for connecting investigators with an interest in the same gene. *Hum Mutat*. 2015;36(10):928–930.
20 Burakov AV, Zhapparova ON, Kovalenko OV, et al. Ste20-related protein kinase LOSK (SLK) controls microtubule radial array in interphase. *Mol Biol Cell*. 2008;19(5):1952–1961.
21 Zhapparova ON, Fokin AI, Vorobyeva NE, Bryantseva SA, Nadezhdina ES. Ste20-like protein kinase SLK (LOSK) regulates microtubule organization by targeting dynactin to the centrosome. *Mol Biol Cell*. 2013;24(20):3205–3214.
22 Fokin AI, Klementeva TS, Nadezhdina ES, Burakov AV. SLK/LOSK kinase regulates cell motility independently of microtubule organization and Golgi polarization. *Cytoskeleton (Hoboken)*. 2016;73(2):83–92.
23 Zamir E, Katz BZ, Aota S, Yamada KM, Geiger B, Kam Z. Molecular diversity of cell-matrix adhesions. *J Cell Sci*. 1999;112(Pt 11):1655–1669.
24 Pankov R, Cukierman E, Katz BZ, et al. Integrin dynamics and matrix assembly: tensin-dependent translocation of alpha(5)beta(1) integrins promotes early fibronectin fibrillogenesis. *J Cell Biol*. 2000;148(5):1075–1090.
25 Menon KP, Carrillo RA, Zinn K. Development and plasticity of the Drosophila larval neuromuscular junction. *Wiley Interdiscip Rev Dev Biol*. 2013;2(5):647–670.
26 Chou VT, Johnson SA, Van Vactor D. Synapse development and maturation at the drosophila neuromuscular junction. *Neural Dev*. 2020;15(1):11.
27 Quach TT, Stratton HJ, Khanna R, et al. Intellectual disability: dendritic anomalies and emerging genetic perspectives. *Acta Neuropathol*. 2021;141(2):139–158.
28 Lei W, Omotade OF, Myers KR, Zheng JQ. Actin cytoskeleton in dendritic spine development and plasticity. *Curr Opin Neurobiol*. 2016;39:86–92.
29 Zamboni V, Jones R, Umbach A, et al. Rho GTPases in intellectual disability: from genetics to therapeutic opportunities. *Int J Mol Sci*. 2018;19(6):1821.
30 Ultanir SK, Yadav S, Hertz NT, et al. MST3 kinase phosphorylates TAO1/2 to enable Myosin Va function in promoting spine synapse development. *Neuron*. 2014;84(5):968–982.
31 Al-Zahrani KN, Baron KD, Sabourin LA. Ste20-like kinase SLK, at the crossroads: a matter of life and death. *Cell Adh Migr*. 2013;7(1):1–10.
32 Swiech L, Blazejczyk M, Urbanska M, et al. CLIP-170 and IQGAP1 cooperatively regulate dendrite morphology. *J Neurosci*. 2011;31(12):4555–4568.
33 Yalgin C, Ebrahimi S, Delandre C, et al. Centrosomin represses dendrite branching by orienting microtubule nucleation. *Nat Neurosci*. 2015;18(10):1437–1445.
34 Pryce BR, Al-Zahrani KN, Dufresne S, et al. Deletion of the Ste20-like kinase SLK in skeletal muscle results in a progressive myopathy and muscle weakness. *Skelet Muscle*. 2017;7(1):3.